Journal of Materials Chemistry A

Accepted Manuscript

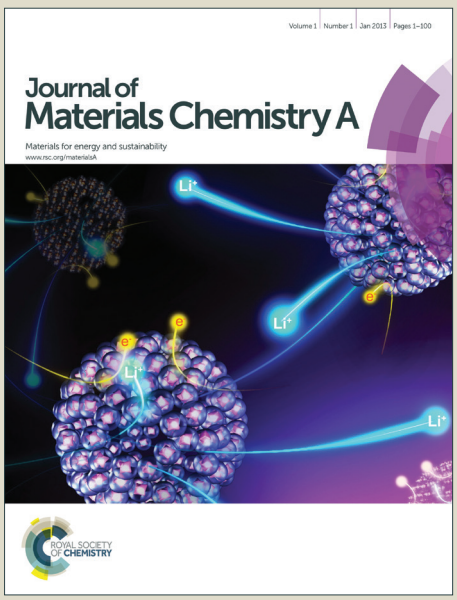

ROYAL SOCIETY OF CHEMISTRY

www.rsc.org/materialsA

Journal Name

ARTICLE

Polyurethane Sponge Facilitating Highly Dispersed TiO_2 Nanoparticles on Reduced Graphene Oxide Sheets for Enhanced Photoelectro-Oxidation of Ethanol †

Received 00th January 20xx,
Accepted 00th January 20xx

DOI: 10.1039/x0xx00000x

www.rsc.org/

Lin Jing,[a, b] Hui Ling Tan,[b] Rose Amal,[b] Yun Hau Ng, [*b] and Ke-Ning Sun[*a]

Three-dimensional (3D) porous polyurethane sponge serves as the sacrificial scaffold for the hydrothermally-synthesized anatase TiO_2-reduced graphene oxide (RGO) composites. The internal channel of the 3D polyurethane structure provides larger exposed TiO_2 seeding and crystal growth area on the pre-adsorbed graphene oxide during the synthesis. The uniform pore size within the polyurethane also prevents severe aggregation of TiO_2 nanoparticles. As a result, TiO_2 nanoparticles are finely dispersed on the RGO sheets. In addition to the general advantages of introducing graphitic carbon to TiO_2 (i.e. hydrophobic carbon for preferential organic adsorption and excellent electron transport of RGO), the presence of polyurethane sponge during the synthesis offers larger contact area between TiO_2 and RGO which is facilitated by the excellent dispersion of TiO_2. Besides, formation of Ti-O-C species is found at the interface and it extends the light absorption of the composite into visible light region. Combining the localized organic adsorption adjacent to TiO_2, efficient charge transfer from large contact area of TiO_2-RGO and the extended light response of the composite, this material demonstrates enhanced photoelectrochemical oxidation of ethanol.

Introduction

Titanium dioxide (TiO_2), as the most widely used semiconductor in photocatalysis and photoelectrocatalysis, has the advantages of availability, high stability, strong photo-oxidizing power, low cost, and environmental friendliness.[1-3] Although high photoactivities have been achieved using bare TiO_2 photocatalyst or photoelectrode, photoexcited charges trapped within TiO_2 network and recombination at the particle interfaces undermine the overall performance of TiO_2.[4,5] The charges recombination is typically more profound when nanoparticles are employed because higher density of particle boundaries exists. Furthermore, UV-only activation of TiO_2 imposed by its wide band gap of 3.2 eV could be an impediment when UV-absent indoor application is relevant.[6, 7] To solve these problems, many strategies have been formulated. For instance, doping elements such as C, N, and S can narrow the bandgap of TiO_2 to extend its light absorption into visible region;[8-10] loading TiO_2 with noble metals such as Au, Pt and Rh as co-catalysts to serve as the catalytic active sites or electron sink for more efficient charge transfer mechanism;[11-13] and integrating TiO_2 with suitable (usually narrower) bandgap semiconductors like WO_3, Bi_2WO_6 and $CuInS_2$ to facilitate extended light absorption and aligned band energy configuration.[14-17] Besides, the combination of TiO_2 with conductive graphitic carbon nanomaterials, particularly reduced graphene oxide (RGO), has been demonstrated to effectively promote charge separation and electron transfer, therefore improving the photocatalytic and photoelectrochemical (PEC) activities.[18-20] In addition, hybridization of TiO_2 with RGO may extend the light response of TiO_2.[21]

Hydrothermal method is an effective way to introduce strong interaction between TiO_2 and RGO induced by the high pressure condition. Owing to RGO's excellent electron conductivity and adjustable hydrophobicity with chemical functionalization, it boosts the photoexcited electron transport and increases the surface-adsorption of organic molecules when RGO is hybridized with TiO_2. This makes RGO-TiO_2 a promising candidate for adsorbing organic molecules on RGO sheets adjacent to the TiO_2 nanoparticles and the subsequent electro-oxidation of the organic species by TiO_2 through a photoelectrochemical way. However, conventional static hydrothermal synthesis non-selectively induced agglomeration of nanoparticles on support materials resulting in undesirable loss of active surface area. In addition to the decrease in surface area, the worsen distribution of nanoparticles on the support also diminished the advantageous functions of the support material, which in the case of RGO-TiO_2 refers to the facilitation of efficient charge extraction from TiO_2 to RGO as

[a] Beijing Key Laboratory for Power Source and Green Catalysis, School of Chemical Engineering and Environment, Beijing Institute of Technology, Beijing, 100081, P. R. China.
Email: bitkeningsun@163.com
[b] Particles and Catalysis Research Group, School of Chemical Engineering, The University of New South Wales, Sydney, NSW, 2052, Australia.
Email: yh.ng@unsw.edu.au

† Electronic Supplementary Information (ESI) available: SEM, TEM, XRD, BET, TGA. See DOI: 10.1039/x0xx00000x

well as the creation of high organic concentration in the microenvironment adjacent to TiO_2. To increase the interfacial contact between TiO_2 and RGO, suppressing the agglomeration of TiO_2 on RGO as well as hindering the restack of RGO during the synthesis are the two strategies recently reported.[22,23]

In this work, with the aims to minimize the agglomeration of TiO_2 on RGO sheets and to strengthen the TiO_2-RGO interactions, we develop a stepwise synthetic route to prepare TiO_2-deposited RGO sheets using a porous polyurethane sponge as template. Nucleation and growth of TiO_2 on RGO sheets took place within the porous polyurethane. The robust three-dimensional structure of polyurethane sponge effectively prevented the restack of RGO sheets and suppressed the agglomeration of TiO_2 nanoparticles on the RGO sheets. The anatase TiO_2 nanoparticles were uniformly grown on RGO sheets. As expected, the obtained sponge-template RGO-TiO_2 (S-RGO-TiO_2), with greatly improved TiO_2 dispersion, large surface area, closer RGO-TiO_2 interaction, and improved absorbance of visible light, showed remarkable enhanced PEC oxidation for aqueous phase ethanol solution.

Experimental Section

Materials

Sponge (polyurethane, PU), titanium (IV) sulphate (Fisher Scientific UK, 15%), ethanol (>98%), deionized water, graphite (Aldrich), sodium nitrate ($NaNO_3$, Univar, 99 %), sulphuric acid (H_2SO_4, Univar, 98 %), potassium permanganate ($KMnO_4$, Fisons, 99.5 %), hydrogen peroxide (H_2O_2, Univar, 30 %).

Preparation of GO

Firstly, 2 g of graphite was reacted with 1 g of $NaNO_3$ in 46 mL of concentrated sulphuric acid at 0 °C by using an ice bath. Secondly, 6 g of $KMnO_4$ was slowly added to the above mixture to obtain a dark green suspension. Then, the suspension was heated at around 40 °C for 2 h. Subsequently, the suspension was diluted using 80 mL of distilled water and 20 mL of 10 % hydrogen peroxide. Lastly, the as-prepared graphene oxide was filtered, washed three times using a mixture of 5 % H_2SO_4 and 5 % H_2O_2 and four times with distilled water, and dried in a vacuum desiccator at room temperature.

Preparation of bare TiO_2

6g $Ti(SO_4)_2$ solution was added in 30 ml deionized water. The solution was sealed and treated at 100 ℃ for 8 h. After reaction, the products was centrifuged, washed and dried at 60 ℃. Then, the sample was annealed at 450 ℃ for 2 h in argon/hydrogen (16:1) atmosphere.

Preparation of S-RGO-TiO_2 and S-RGO

50 mg GO was firstly dispersed in 20 mL ethanol under ultrasonic treatment for 30 min. The sponge (15 mm × 15 mm × 15 mm) was immersed in the GO solution to adsorb enough GO into the porous structure. Then, the sponge was dried at 60 ℃ to remove the ethanol in the sponge. The above processes were repeated until all of the GO was absorbed inside of the sponge. Then, the obtained GO-sponge was immersed in 30 ml deionized water contain 6 g $Ti(SO_4)_2$ solution, sealed and treated at 100 ℃ for 5 h. The sponge was washed carefully with deionized water and dried at 60 ℃. Lastly, the sponge was removed by annealing at 450 ℃ for 2 h in argon/hydrogen (16:1) atmosphere to obtain the S-RGO-TiO_2 with sponge-like 3D structure. The photographs of the detailed synthetic procedure of S-RGO-TiO_2 are shown in Fig. S1. For comparison, the sponge template RGO (S-RGO) and the template-free RGO-TiO_2 were also obtained in the same procedure without the growth of TiO_2 and adsorption process, respectively.

Structural and morphological characterization

The morphological features of the TiO_2, RGO-TiO_2 and S-RGO-TiO_2 were characterized by transmission electron microscopy (TEM, Tecnai). SEM images of bare sponge, GO-sponge and GO-TiO_2-sponge were characterized by SEM-3400i. Raman spectra of TiO_2, GO, RGO-TiO_2 and S-RGO-TiO_2 were performed on inVia Raman spectrometer with 514 nm excitation. FTIR (Spotlight 400) of bare sponge, GO, S-RGO and S-RGO-TiO_2 were carried out in the transmittance mode in the spectral range 650-2500 cm^{-1} with a resolution better than 0.1 cm^{-1}. X-ray powder diffraction (XRD) patterns of anatase TiO_2, RGO-TiO_2 and S-RGO-TiO_2 were taken on XRD-MPD-Scherrer using Cu K α irradiation in the 2ϑ range from 20° to 70°. Thermogravimetric analysis (TGA) of RGO-TiO_2 and S-RGO-TiO_2 was performed under air using TA TGA Q5000. The samples were heated from room temperature to 800 °C at 10 °C min^{-1}. Brunauer-Emmett-Teller (BET) measurements of RGO-TiO_2 and S-RGO-TiO_2 were performed on Micrometric Tristar 3000 system using nitrogen adsorption. UV-vis spectra of bare TiO_2, RGO-TiO_2, and S-RGO-TiO_2 were recorded using Shimadzu UV-3600 spectrometer. Photoluminescence spectra (PL) of TiO_2 (2.0 mg), RGO-TiO_2 (2.4 mg) and S-RGO-TiO_2 (3.3 mg) were acquired at room temperature using a Fluoromax-4 spectrophotometer in diffuse reflection mode and with an excitation wavelength of 330 nm. X-ray photoelectron spectroscopy (XPS) of bare TiO_2, RGO-TiO_2 and S-RGO-TiO_2 were conducted on an Escalab250Xi spectrometer (Thermo Scientific, UK).

PEC measurements

The working electrodes were prepared as follows: The bulk S-RGO-TiO_2 was firstly ground to fine powder. 2 mg of the TiO_2, RGO-TiO_2 and S-RGO-TiO_2 were dispersed in 1 mL ethanol respectively, by sonication for 30 min to obtain homogeneous suspension. Then, the samples were loaded onto the FTO electrodes (1.5×1.5 cm squares) and dried in oven at 100 ℃ for 1h. All photocurrent and electrochemical experiments were performed with an Autolab potentiostat (Model PGSTAT302N) and conducted in a 0.5 M Na_2SO_4 and 0.1 M ethanol electrolyte solution using the three-electrode setup. The photocurrent was measured for each switch on/off event with a bias voltage of 0.25 V under the UV-visible light irradiation. Light illumination was provided by a 300 W Xe lamp (PerkinElmer, CERMAX, LC-300BUV). Linear sweep

voltammetry (LSV) was also recorded with a sweeping rate of 1 mV/s in the potential range of -0.4 to 0.8 V with light chopping every 20 seconds.

Results and discussion

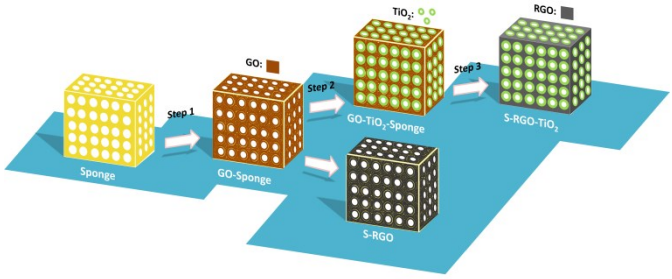

Scheme 1. Illustration of the stepwise synthetic procedure of S-RGO-TiO_2 and S-RGO. Step 1, 2 and 3 represent adsorption of GO, hydrothermal treatment and annealing treatment, respectively.

The stepwise synthetic procedure of S-RGO-TiO_2 is illustrated in Scheme 1. First, the polyurethane sponge was used as the host to adsorb graphene oxide (GO, precursor of RGO) sheets. As can be seen in Fig. S1a and b, the color of polyurethane sponge turned from yellow to dark brown upon immersion in the 2.5 g/L GO solution, which implied the successful coating of GO on the polyurethane. Scanning electron microscope (SEM) images of the bare polyurethane sponge and GO-adsorbed sponge (GO-sponge) in Fig. S2a and b indicated the evenly distributed GO sheets within the pores of polyurethane sponge. Subsequently, the pre-adsorbed GO-sponge was subjected to hydrothermal treatment at 100 ℃ in the presence of $Ti(SO_4)_2$ as the precursor for TiO_2. After the hydrothermal treatment, small particles were clearly observed on the GO sheets as shown in Fig. S2c, which suggested the successful introduction of TiO_2 particles on the surface of GO sheets within the polyurethane sponge. The obtained GO-TiO_2-sponge was annealed at 450 ℃ for 2 h in argon/hydrogen (16:1) atmosphere to remove the polyurethane sponge template and to reduce the GO to RGO.[24,25] Finally, a sponge-like RGO-TiO_2 (S-RGO-TiO_2) block was obtained. For comparison, the preparation of sponge-template RGO (S-RGO) was prepared through the simultaneous GO reduction and polyurethane removal as shown in Scheme 1. Bare polyurethane sponge was also annealed under the same condition and it was completely removed, indicated the effectiveness of template removal upon annealing.[26] The photographs of bare polyurethane sponge, S-RGO and S-RGO-TiO_2 are shown in Fig. S3. Compared to the black S-RGO, the color of S-RGO-TiO_2 was grey, implying the existence of TiO_2 on RGO sheets.

Kinetics of the morphological evolution of TiO_2 nanoparticles on RGO sheets provides information on the likelihood of the charge interaction between the two components. S-RGO-TiO_2 samples obtained with different time of hydrothermal treatment were monitored by transmission electron microscopy (TEM) as shown in Fig. 1a-f. Compared with the clean surface of bare S-RGO sheets (Fig. 1a), tiny nanoparticles started to be observed on the RGO sheets with 1h and 2h hydrothermal treatment (Fig. 1b, c). With the time increased to 4 h and 5 h (Fig. 1d, e), the coverage of the nanoparticles on RGO sheets was comprehensive with more nanoparticles evenly distributed across the RGO sheets. These nanoparticles were identified as anatase TiO_2 using x-ray diffraction (XRD). Extended reaction length of 7 h, however, inevitably induced agglomeration of TiO_2 nanoparticles on the RGO sheets though the primary particle size remain relatively unchanged (Fig. 1f). Bare TiO_2 and template-free TiO_2 modified RGO (RGO-TiO_2) samples obtained with 5 h hydrothermal treatment were also prepared for comparison (Fig. S4). In these samples, the TiO_2 component appeared as large clusters consist of fused nanoparticles. These observations reflect the constructive effect of porous polyurethane sponge in suppressing severe agglomeration of TiO_2 on RGO sheets.

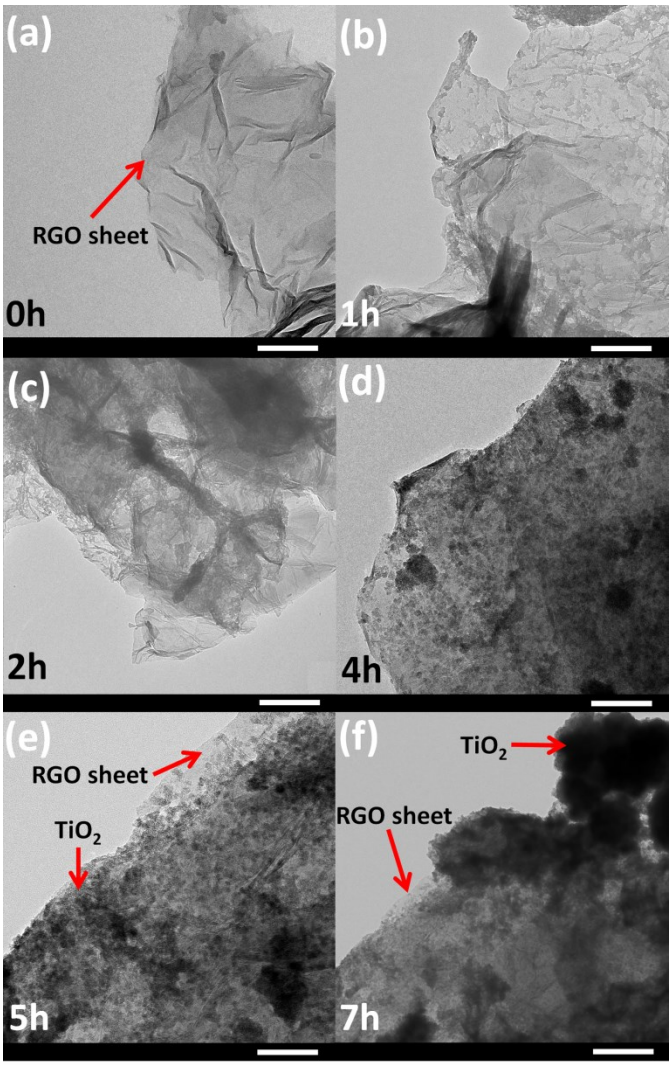

Fig. 1 TEM images of S-RGO sheets (a) and S-RGO-TiO_2 obtained with different time of hydrothermal treatment: (b) 1h, (c) 2h, (d) 4h, (e) 5h, and (f) 7h. Scale bar: 200 nm.

To understand the crucial role of sponge template in controlling the morphology of TiO_2 modified RGO, different morphological features of TiO_2-deposited RGO sheets prepared with and without polyurethane sponge template are illustrated in Scheme 2. In the absence of polyurethane sponge template, GO sheets sank immediately during the hydrothermal reaction. In this typical static hydrothermal reaction, TiO_2 nanoparticles were therefore mainly nucleated and deposited on the upper layer of the bulk GO precipitation

after 5 h hydrothermal treatment. In fact, TEM analysis of this sample revealed that a large portion of the RGO sheets were undecorated with TiO_2. In addition, severe agglomeration of TiO_2 on the surface of RGO sheets and the resultant irregular-shaped TiO_2 clusters were observed, as shown in the inset TEM image of Scheme 2b. In the polyurethane sponge system, GO sheets were adsorbed on the internal and external surface of the porous polyurethane. The GO sheets were kept exfoliated and distributed within the robust sponge framework during the nucleation and growth of TiO_2 in hydrothermal condition (Scheme 2c). Therefore, higher density of nucleated sites was available on RGO sheets to facilitate the growth of TiO_2 nanoparticles, as illustrated in Scheme 2d. As a result, homogeneous TiO_2-deposited RGO sheets were obtained. The inset TEM image in Scheme S1d shows an improved dispersion of TiO_2 nanoparticles on RGO sheets as compared to the sponge-free RGO-TiO_2 sample.

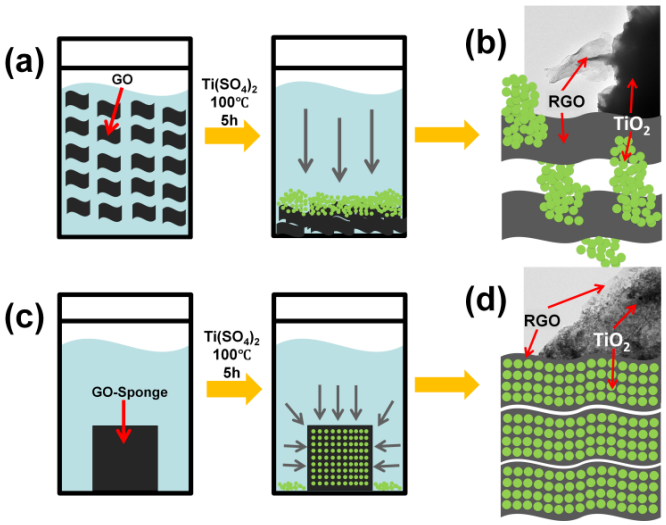

Scheme 2. (a) Illustration of the growth of TiO_2 nanoparticles on GO sheets without polyurethane sponge template during the hydrothermal process. (b) Morphological structure of TiO_2-deposited RGO sheets obtained without the polyurethane sponge template after the annealing treatment. (c) Illustration of the growth of TiO_2 nanoparticles on GO sheets with polyurethane sponge template during the hydrothermal process. (d) Morphological structure of TiO_2 modified RGO sheets obtained with the polyurethane sponge template after the annealing treatment.

To confirm the successful reduction of GO to RGO and the introduction of anatase TiO_2 nanoparticles on the surface of RGO sheets, Raman and Fourier transform infrared spectroscopy (FTIR) were first characterized. In Fig. 2a, Raman spectrum of S-RGO-TiO_2 shows the typical mode of anatase TiO_2 (150, 203, 388, 503, and 622 cm^{-1}) and RGO with the presence of a D band at 1349 cm^{-1} and a G band at 1580 cm^{-1}. The D band is corresponding to the sp^3 defect, while G band is a common feature of the graphitic sp^2 carbon. The ratio of the intensity of the D band to that of the G band (I_D/I_G) indicates the degree of disorder from graphite structure. It is obvious that both S-RGO-TiO_2 and S-RGO had increased I_D/I_G of 1.21 and 1.24, respectively, compared to that of GO (0.93). This increased I_D/I_G ratio is used as an indicator of the reduction of GO because the deoxygenation (reduction mode) of GO by annealing is commonly associated with the introduction of more defects at the edge of the graphitic sheets.[27] Correspondingly, G band for both S-RGO-TiO_2 and S-RGO shifted to lower frequency as the ratio of sp^3/sp^2 increased after reduction of GO.[28,29] FTIR spectra of the bare polyurethane sponge, GO, S-RGO and S-RGO-TiO_2 are shown in Fig. 2b. The peak at 1715 cm^{-1} attributed to C=O stretching mode was disappeared for S-RGO-TiO_2 sample compared to GO, while new peaks below 1000 cm^{-1} appeared corresponding to the stretching vibration of Ti–O–Ti bonds in crystalline TiO_2.[30] In addition, two new peaks at 1047 and 1120 cm^{-1} were observed for the formation of Ti-O-C bonds between TiO_2 and RGO.[31,32] These results strongly demonstrate the successful reduction of GO and the combination of TiO_2 nanoparticles with the RGO sheets. Moreover, the peaks (from 650 to 1800 cm^{-1}) observed in bare polyurethane sponge were absent for both S-RGO and S-RGO-TiO_2, indicating that the sponge template were thoroughly removed during the annealing process.

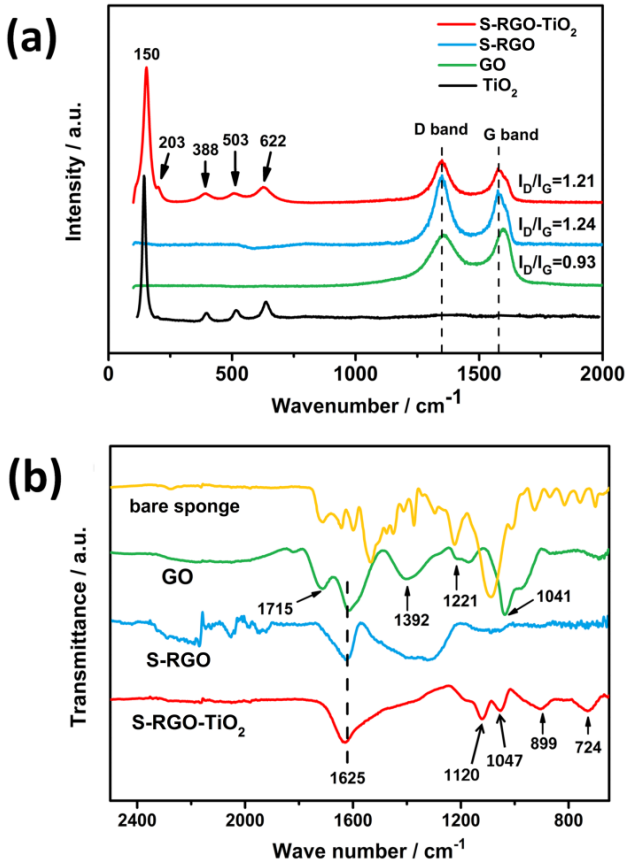

Fig. 2 (a) Raman spectra of TiO_2, GO, S-RGO, and S-RGO-TiO_2. (b) FTIR spectra of bare sponge, GO, S-RGO and S-RGO-TiO_2.

The crystallographic structure of bare TiO_2, RGO-TiO_2 and S-RGO-TiO_2 was further characterized by XRD as shown in Fig. S5. All samples exhibited XRD peaks corresponding to the (101), (004), (200), (105), (211) and (204) planes for the anatase structure of TiO_2. Large surface area of this composite material is crucial for creating a localized high organic concentration microenvironment adjacent to TiO_2. Nitrogen isotherm adsorption-desorption curves of RGO-TiO_2 and S-RGO-TiO_2 were performed and shown in Fig. S6. The presence of small volume of mesopores with wide range of pore size (< 5 nm) observed in the S-RGO-TiO_2 was generated upon the thermal removal of sponge. In contrast, these mesopores were absent in RGO-TiO_2 sample. As expected, from the Brunauer-Emmett-

Teller (BET) results, the surface area of S-RGO-TiO_2 (137 m^2g^{-1}) was much greater than that of RGO-TiO_2 (12 m^2g^{-1}), suggesting that S-RGO-TiO_2 could provide more adsorption sites for organic molecules and dispersion sites for TiO_2 nanoparticles to facilitate efficient PEC reaction.[33,34] The low surface area of RGO-TiO_2 was mainly due to the agglomeration of TiO_2 and RGO sheets during the hydrothermal treatment and annealing process without the sponge template.

The mass content of RGO in RGO-TiO_2 and S-RGO-TiO_2 was evaluated by TGA, respectively. TGA curves (Fig. S7) of both RGO-TiO_2 and S-RGO-TiO_2 showed weight loss from room temperature to 150 °C which was caused by desorption of physically absorbed water. In addition, the obvious weight loss from 150 to 600 °C was attributed to the decomposition of the carbon skeleton of RGO in the composites. As a result, the RGO mass ratios for RGO-TiO_2 and S-RGO-TiO_2 are 17.8 and 40.8 wt%, respectively, which are calculated from the weight loss between 150 and 800 °C.

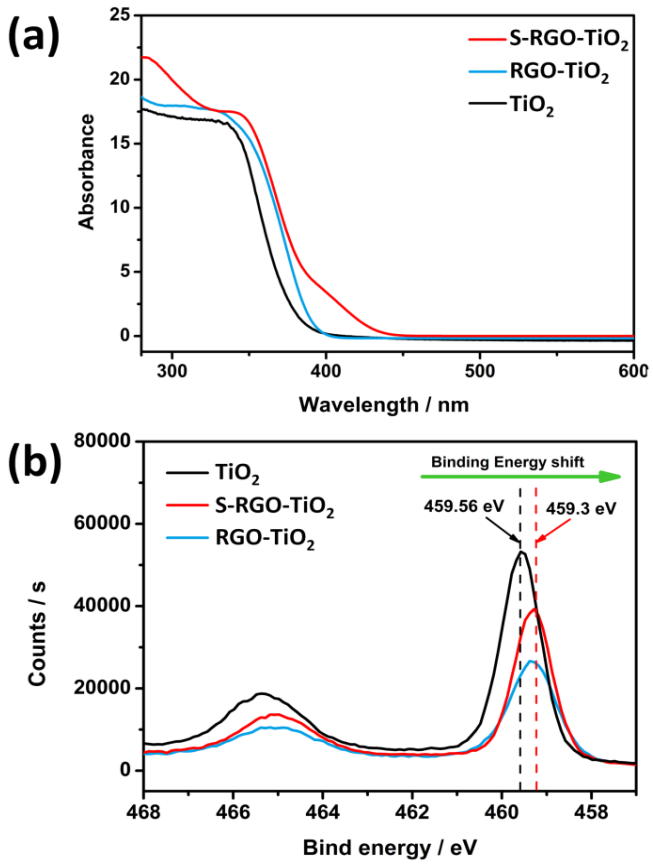

Fig. 3 (a) UV-Vis spectra and (b) XPS spectra of TiO_2, RGO-TiO_2 and S-RGO-TiO_2

Fig. 3a shows the UV-vis spectra of TiO_2, RGO-TiO_2 and S-RGO-TiO_2. Compared to the bare TiO_2, an obvious red shift of 50 nm and a relatively weak red shift in the absorption edge were observed for the S-RGO-TiO_2 and RGO-TiO_2, respectively. The red shift and the improved light absorption for both S-RGO-TiO_2 and RGO-TiO_2 can be attributed to the formation of surface Ti-O-C species as indicated in the Ti 2p XPS (Fig. 3b).[35] Compared to the binding energy of bare TiO_2, both RGO-TiO_2 and S-RGO-TiO_2 presented a negative shift of 0.26 eV from 459.56 eV to 459.3 eV, suggesting the formation of Ti-O-C bonds between the surface TiO_2 and RGO. In addition, annealing at 450 ℃ is a suitable temperature for the formation of Ti-O-C species between TiO_2 and RGO.[36] For S-RGO-TiO_2, the enlarged contact area between TiO_2 and RGO can improve the formation of Ti-O-C species between TiO_2 and RGO, resulting in improved visible light absorption. Note that the negative shift in Ti 2p XPS spectrum is unlikely caused by the changes of particle size of TiO_2 or the adsorbed water on TiO_2. This is because the primary particle size of TiO_2 was unchanged upon modification (TEM images) while water-adsorbed TiO_2 could not yield extension of light absorption (UV-Vis spectrum). For RGO-TiO_2, the severe agglomeration of TiO_2 further reduced the contact area between TiO_2 and RGO. Therefore, even with the existence of Ti-O-C species in RGO-TiO_2, it is insufficient to yield the significant red shift to visible light region as compared to S-RGO-TiO_2.

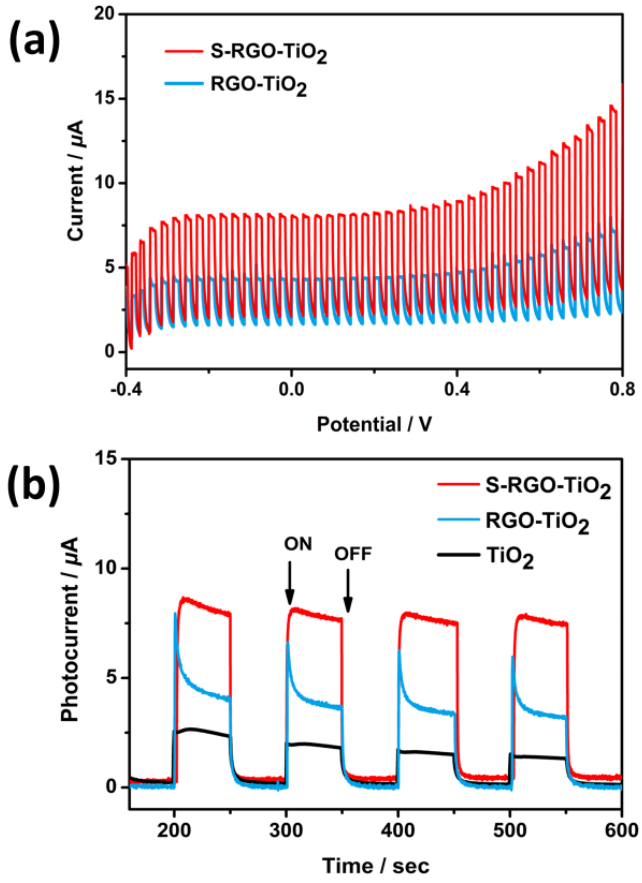

Fig. 4 (a) Current-voltage curves of RGO-TiO_2 and S-RGO-TiO_2 electrodes in 0.5 M Na_2SO_4 and 0.1 M ethanol electrolyte solution under UV-visible light irradiation at a scan rate of 1mV/s, (b) amperometric photocurrent responses of TiO_2, RGO-TiO_2, and S-RGO-TiO_2 at 0.25 V in 0.5 M Na_2SO_4 and 0.1 M ethanol electrolyte solution under UV-visible light.

Subsequently, powders of all samples (TiO_2, RGO-TiO_2 and S-RGO-TiO_2) were made into electrodes for PEC evaluation. Current-voltage curves of all electrodes were measured in 0.5 M Na_2SO_4 and 0.1 M ethanol electrolyte solution. Upon light irradiation, the photocurrent increased with the applied potential (Fig. 4a). S-RGO-TiO_2 electrode generated much higher photocurrent than that of the RGO-TiO_2 electrode, implying that the improved dispersion of the fine TiO_2 nanoparticles and its associated enlarged contact area

between TiO_2 and RGO have assisted the photocharge transportation with higher efficiency. Besides, the extended light absorption to 450 nm (Fig. 3a) may also contribute to the improved photocurrent of S-RGO-TiO_2. The amperometric current-time curves of TiO_2, RGO-TiO_2 and S-RGO-TiO_2 electrodes further verify the reproducibility and the stability of the photocurrent generation (Fig. 4b). Under the UV-visible light, all three electrodes exhibited instantaneous current responses to each illumination on/off cycles. Clearly, photocurrent obtained on RGO-TiO_2 and S-RGO-TiO_2 electrodes were two- and five-fold of the TiO_2 electrode respectively, indicating that the PEC oxidation of ethanol was effectively improved attributed to the combination of RGO and TiO_2. Under visible light irradiation (λ > 400 nm), no obvious photocurrent was observed on TiO_2 electrode (Fig. S8). In contrast, weak photocurrent and strong photocurrent responses were observed on RGO-TiO_2 and S-RGO-TiO_2 electrodes respectively. The results match well with the UV-vis spectra in Fig. 3a.

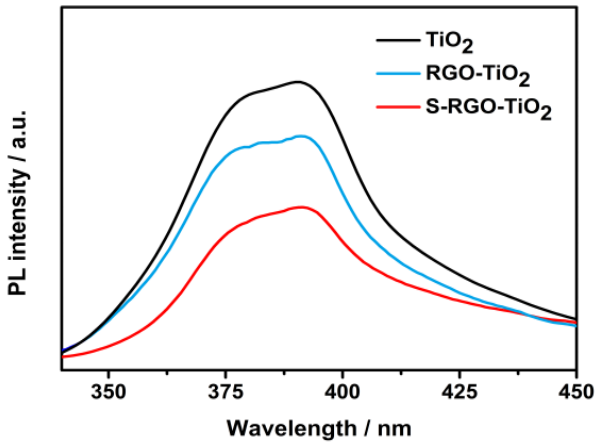

Fig. 5 PL spectra of TiO_2, RGO-TiO_2, and S-RGO-TiO_2.

The well dispersed TiO_2 nanoparticles on RGO sheets with maximized contact area for electron transfer would suppress the charge recombination. The severity of charge recombination can be measured by evaluating the emission of luminescent radiation when the excited electrons return to their ground state. The photoluminescence (PL) spectra of TiO_2, RGO-TiO_2 and S-RGO-TiO_2 are shown in Fig. 5. In comparison, the PL peak of S-RGO-TiO_2 was the weakest, indicating the homogenous distribution of TiO_2 on RGO sheets boosted the electron transfer from the excited TiO_2 to RGO sheets and thus less charge recombination was observed.

Based on the above systematic analysis, we proposed a mechanism to understand the enhanced PEC ethanol oxidation on S-RGO-TiO_2. As illustrated in Scheme 3, the PEC ethanol oxidation performance of S-RGO-TiO_2, RGO-TiO_2 and TiO_2 can be mainly affected by the following three steps. In **step 1**, both S-RGO-TiO_2 and RGO-TiO_2 can adsorb more ethanol molecules from the solution due to the hydrophobicity of the RGO sheets.[37,38] Compared with RGO-TiO_2, S-RGO-TiO_2 sample with large surface area can adsorb more ethanol molecules, which should increase the ethanol molecule concentration in the micro-environment of TiO_2 surface. RGO has been demonstrated to have the affinity towards small organic molecules (acetone, acetonitrile, dichloromethane, ethanol, ethyl acetate, hexane, and toluene) adsorption.[39] We believe that the high ethanol molecules concentration is an essential factor for the enhanced photocurrent. Under the light irradiation, electrons are excited from the valence band (VB) to the conduction band (CB) of TiO_2 to generate electron-hole pairs. For bare TiO_2 sample, the holes on the VB of TiO_2 can be consumed for the oxidation of ethanol in the solution (**step 2**), while the photo-induced electrons on CB of TiO_2 can be transferred to the fluorine-doped tin oxide (FTO) electrode (**step 3**). In the presence of RGO, more photo-induced electrons on the CB of TiO_2 can be transferred to the FTO electrode via the conductive RGO than that of the bare TiO_2, resulting in efficient charge separation and holes consumption for ethanol oxidation. This property is further enhanced in the case of S-RGO-TiO_2. Owing to the smaller and better distributed TiO_2, effective contact area between TiO_2 and RGO is larger. This then promotes a more efficient transfer of photo-induced electrons in CB of TiO_2 to RGO in comparison to RGO-TiO_2.

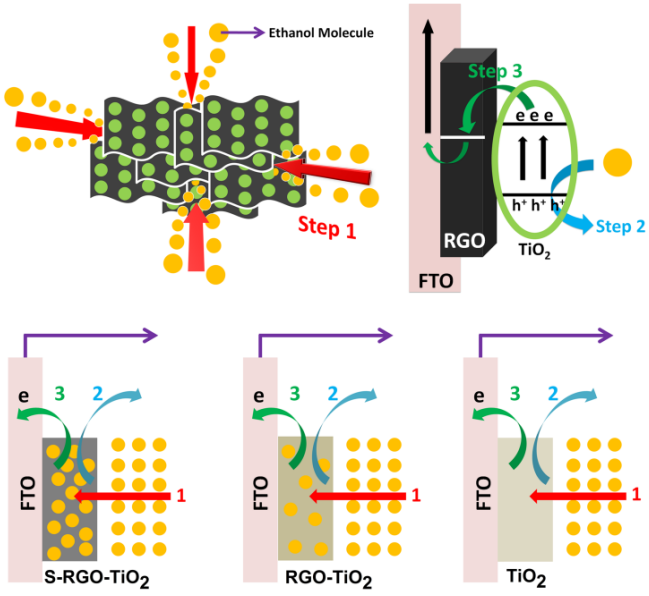

Scheme 3. Proposed PEC process mechanism of ethanol oxidation and electron transfer at different electrodes.

Conclusions

In conclusion, we have demonstrated a simple, low cost and controllable strategy to prepare TiO_2-deposited RGO sheets. Three-dimensional porous polyurethane sponge was used as a template for the first time to control the morphological structure of TiO_2 deposited RGO sheets, afforded a homogenous deposition of small TiO_2 nanoparticles on RGO sheets. The resulted photocatalyst composite showed extended light absorption into visible region and enhanced PEC ethanol oxidation performance, exhibiting two- and five-fold photocurrent of the polyurethane sponge-free RGO-TiO_2 and bare TiO_2, respectively, under identical experimental conditions. Such an enhanced PEC activity is believed to

attribute to the synergistic effect between TiO_2 and RGO. The presence of polyurethane template during the synthesis facilitated better dispersion of TiO_2 on RGO sheets. A better dispersion of TiO_2 on RGO could (1) effectively improve the formation of Ti-O-C between TiO_2 and RGO (as supported by Ti 2p XPS), resulting in extended light absorption range; (2) promote the electrons transfer between TiO_2 and RGO, i.e. less charge recombination as evidenced by PL spectroscopy; and (3) increase the surface area with more active sites for the ethanol oxidation (as shown by BET analysis). This work offers insights into the design of functional materials with controllable properties for electrocatalysis, photocatalysis and photoelectrocatalysis.

Acknowledgements

This work was financially supported by the Australia Research Council Discovery Project (DP 110101638) and partially supported from the China Scholarship Council (CSC, no. 201406030034). The authors appreciate the facility and technical assistances supported by UNSW Mark Wainwright Analytical Centre. In particular, Dr. Bill Gong from Solid State & Elemental Analysis Unit of UNSW for his help in XPS measurement and analysis.

Notes and references

1 D. Chen, F. Huang, Y.-B. Cheng and R. A. Caruso, *Adv. Mater.*, 2009, **21**, 2206.
2 X. Zheng, D. Yu, F.-Q. Xiong, M. Li, Z. Yang, J. Zhu, W.-H. Zhang and C. Li, *Chem. Commun.*, 2014, **50**, 4364.
3 J.-H. Yun, Y. H. Ng, C. Ye, A. J. Mozer, G. G. Wallace and R. Amal, *ACS Appl. Mater. Interfaces*, 2011, **3**, 1585.
4 L. Jing, M. Wang, X. Li, R. Xiao, Y. Zhao, Y. Zhang, Y.-M. Yan, Q. Wu and K. Sun, *Appl. Catal. B: Environ.*, 2015, **166**, 270.
5 H. C. Leventis and S. A. Haque, *Energy Environ. Sci.*, 2009, **2**, 1176.
6 L. Jing, Z.-Y. Yang, Y.-F. Zhao, Y.-X. Zhang, X. Guo, Y.-M. Yan and K.-N. Sun, *J. Mater. Chem. A*, 2014, **2**, 1068.
7 J. S. Lee, K. H. You and C. B. Park, *Adv. Mater.*, 2012, **24**, 1084.
8 Y. Park, W. Kim, H. Park, T. Tachikawa, T. Majima and W. Choi, *Appl. Catal. B: Environ.*, 2009, **91,** 355.
9 J. Ananpattarachai, P. Kajitvichyanukul and S. Seraphin, *J. Hazard. Mater.*, 2009, **168,** 253.
10 X. B. Chen and C. Burda, *J. Am. Chem. Soc.*, 2008, **130**, 5018.
11 X. Z. Li and F. B. Li, *Environ. Sci. Technol.*, 2001, **35,** 2381.
12 T. Chen, Z. H. Feng, G. P. Wu, J. Y. Shi, G. J. Ma, P. L. Ying and C. Li, *J. Phys. Chem. C*, 2007, **111,** 8005.
13 H. Einaga, T. Ibusuki and S. Futamura, *Environ. Sci. Technol.*, 2004, **38,** 285.
14 Y. T. Kwon, K. Y. Song, W. I. Lee, G. J. Choi and Y. R. Do, *J. Catal.*, 2000, **191,** 192.
15 Q. C. Xu, Y. H. Ng, Y. Zhang, J. S. C. Loo, R. Amal and T. Timothy Thatt Yang, *Chem. Commun.*, 2011, **47,** 8641.
16 J.-H. Yun, Y. H. Ng, S. Huang, G. Conibeer and R. Amal, *Chem. Commun.*, 2011, **47,** 11288.
17 M. Jung, J. Scott, Y. H. Ng, Y. Jiang and R. Amal, *Int. J. Hydrogen Energ.*, 2014, **39,** 12499.
18 Y. H. Ng, S. Ikeda, M. Matsumura and R. Amal, *Energy Environ. Sci.*, 2012, **5**, 9307.
19 N. J. Bell, Y. H. Ng, A. Du, H. Coster, S. C. Smith and R. Amal, *J. Phys. Chem. C*, 2011, **115**, 6004.
20 Y. H. Ng, A. Iwase, N. J. Bell, A. Kudo and R. Amal, *Catal. Today*, 2011, **164**, 353.
21 Y. Zhang and C. Pan, *J. Mater. Sci.*, 2011, **46**, 2622.
22 Y. Zhang, N. Zhang, Z.-R. Tang and Y.-J. Xu, *Phys. Chem. Chem. Phys.*, 2012, **14**, 9167.
23 W. Tu, Y. Zhou, Q. Liu, S. Yan, S. Bao, X. Wang, M. Xiao and Z. Zou, *Adv. Funct. Mater.*, 2013, **23**, 1743.
24 C. Valles, J. D. Nunez, A. M. Benito and W. K. Maser, *Carbon*, 2012, **50**, 835.
25 Z.-Y. Yang, L.-J. Jin, G.-Q. Lu, Q.-Q. Xiao, Y.-X. Zhang, L. Jing, X.-X. Zhang, Y.-M. Yan and K.-N. Sun, *Adv. Funct. Mater.*, 2014, **24**, 3917.
26 R. Bilbao, J. F. Mastral, J. Ceamanos and M. E. Aldea, *J. Anal. Appl. Pyrolysis*, 1996, **37**, 69.
27 J.-H. Yun, Y. H. Ng, R. J. Wong and R. Amal, *ChemCatChem*, 2013, **5**, 3060.
28 D. Beeman, J. Silverman, R. Lynds and M. R. Anderson, *Phys. Rev. B*, 1984, **30**, 870.
29 A. Richter, H. J. Scheibe, W. Pompe, K. W. Brzezinka and I. Muhling, *J. Non-Cryst. Solids*, 1986, **88**, 131.
30 H. Zhang, X. J. Lv, Y. M. Li, Y. Wang and J. H. Li, *ACS Nano*, 2010, **4**, 380.
31 M. J. Velasco, F. Rubio, J. Rubio and J. L. Oteo, *Spectrosc. Lett.*, 1999, **32**, 289.
32 G. Lui, J.-Y. Liao, A. Duan, Z. Zhang, M. Fowler and A. Yu, *J. Mater. Chem. A*, 2013, **1**, 12255.
33 Y. H. Ng, S. Ikeda, T. Harada, S. Higashida, T. Sakata, H. Mori and M. Matsumura, *Adv. Mater.*, 2007, **19**, 597.
34 Y. H. Ng, S. Ikeda, T. Harada, Y. Morita and M. Matsumura, *Chem. Commun.*, 2008, **27**, 3181.
35 J.-H. Yun, R. J. Wong, Y. H. Ng, A. Du and R. Amal, *RSC Adv.*, 2012, **2**, 8164.
36 O. Akhavan and E. Ghaderi, *Nanoscale*, 2013, **5**, 10316.
37 N. Duc Dung, N.-H. Tai, S.-B. Lee and W.-S. Kuo, *Energy Environ. Sci.*, 2012, **5**, 7908.
38 Y. Liu, J. Ma, T. Wu, X. Wang, G. Huang, Y. Liu, H. Qiu, Y. Li, W. Wang and J. Gao, *ACS Appl. Mater. Interfaces*, 2013, **5**, 10018.
39 P. Lazar, F. Karlicky, P. Jurecka, M. Kocman, E. Otyepkova, K. Safarova and M. Otyepka, *J. Am. Chem. Soc.*, 2013, **135**, 6372.

Polyurethane Sponge Facilitating Highly Dispersed TiO_2 Nanoparticles on Reduced Graphene Oxide Sheets for Enhanced Photoelectro-Oxidation of Ethanol

Lin Jing,[1, 2] *Hui Ling Tan,*[2] *Rose Amal,*[2] *Yun Hau Ng,* [*2] *and Ke-Ning Sun*[*1]

1. Beijing Key Laboratory for Chemical Power Source and Green Catalysis,School of Chemical Engineering and Environment,Beijing Institute of Technology, Beijing 100081, People's Republic of China

2. Particles and Catalysis Research Group, School of Chemical Engineering, The University of New South Wales, Sydney NSW 2052, Australia

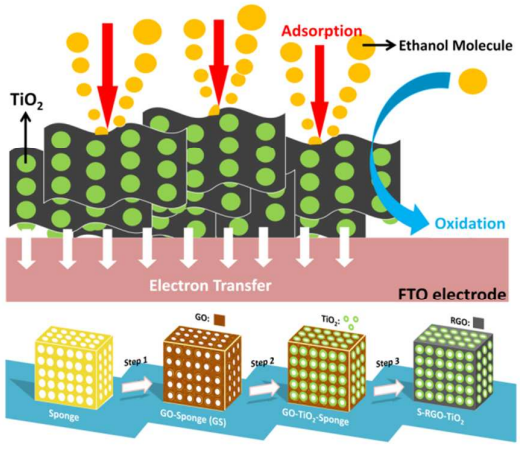

Sponge-template TiO_2-reduced graphene oxide (RGO) is prepared with improved dispersion of TiO_2 on RGO sheets for efficient photoeletro-oxidation of ethanol.